Direct Imaging of Transient Fano Resonances in N_2 Using Time-, Energy-, and Angular-Resolved Photoelectron Spectroscopy

Martin Eckstein,[1] Chung-Hsin Yang,[1] Fabio Frassetto,[2] Luca Poletto,[2] Giuseppe Sansone,[3] Marc J. J. Vrakking,[1] and Oleg Kornilov[1,*]

[1]*Max Born Institute, Max-Born-Straße 2A, 12489 Berlin, Germany*

[2]*National Research Council—Institute of Photonics and Nanotechnologies (CNR-IFN), via Trasea 7, I-35131 Padova, Italy*

[3]*Dipartimento di Fisica, Politecnico, Piazza Leonardo da Vinci 32, 20133 Milano, Italy*

(Received 29 November 2015; published 20 April 2016)

Autoionizing Rydberg states of molecular N_2 are studied using time-, energy-, and angular-resolved photoelectron spectroscopy. A femtosecond extreme ultraviolet pulse with a photon energy of 17.5 eV excites the resonance and a subsequent IR pulse ionizes the molecule before the autoionization takes place. The angular-resolved photoelectron spectra depend on pump-probe time delay and allow for the distinguishing of two electronic states contributing to the resonance. The lifetime of one of the contributions is determined to be 14 ± 1 fs, while the lifetime of the other appears to be significantly shorter than the time resolution of the experiment. These observations suggest that the Rydberg states in this energy region are influenced by the effect of interference stabilization and merge into a complex resonance.

DOI: 10.1103/PhysRevLett.116.163003

States undergoing electronic autoionization belong to one of the simplest classes of states displaying multielectron dynamics. They are electronically excited states of the neutral atom or molecule at an energy above the ionization threshold. Electron rearrangement can lead to the decay of such a state and the emission of an electron, i.e., ionization. In absorption experiments autoionizing states lead to Fano profiles, which originate from interference between the autoionization and direct ionization channels [1].

Non-time-resolved, frequency-domain methods, such as photoelectron spectroscopy at a fixed photon energy or energy-resolved spectroscopies such as threshold or zero-kinetic-energy photoelectron spectroscopy, often cannot directly distinguish molecular autoionizing states from vibrational progressions. The possibility of performing a lifetime analysis is limited in these methods to lines with simple profiles, and becomes prohibitively complex for overlapping and interacting resonances. Time-resolved methods overcome these drawbacks. In a time-resolved experiment, the autoionizing state can be excited by a first pulse [typically an extreme ultraviolet (XUV) pulse] and then ionized by a second probe pulse arriving with a delay smaller than the lifetime of that state. Such experiments have been performed for several atomic targets [2–4]. Here we present the first direct imaging of molecular Fano resonances in nitrogen using time-, energy-, and angular-resolved photoelectron spectroscopy [5].

In 1930 Hopfield discovered that the XUV absorption spectrum of nitrogen below the ionization threshold of the $B^2\Sigma_u^+$ state contains many sharp resonances [6]. They originate from Rydberg series converging to the $B^2\Sigma_u^+$ threshold. Hopfield identified two series of resonances in his experiments, which he called the absorption and "emission" series. In 1962 Ogawa and Tanaka suggested a third series, which is adjacent to the Hopfield emission series of states [7]. However, later Huber *et al.* challenged this assignment based on experiments with N_2 in molecular beams. They demonstrated that the resonances assigned by Ogawa and Tanaka disappear when the N_2 molecules are rotationally cold [8].

Despite the large body of available data [9–14], reliable assignment of the observed features remains difficult. Even for high-resolution spectroscopy, assignment of the lower Rydberg states is complicated by rich structures associated with vibrational progressions of lower cationic states [15], whereas higher Rydberg states were found to be strongly influenced by rotations of the molecule [8]. The most complete calculations to date are those of Raoult *et al.* [16], who assign the Hopfield absorption series to $(B^2\Sigma_u^+)n'd'\sigma_g$ states, where quotes denote that d is the dominant component of the $s + d$ Rydberg supercomplex [16]. The emission series is assigned to $nd\pi_g$ Rydberg states with possible contributions of $n's'\sigma_g$ states.

Here, for the first time, we apply time-resolved methods to unravel the dynamics of autoionization at one of the N_2 resonances. We use a recently constructed time-delay-compensating monochromator beam line [5] to excite nitrogen molecules with an XUV pulse with a photon energy centered at 17.5 eV. Absorption of XUV photons leads both to direct ionization and excitation of a member of the Hopfield emission series. The molecule is ionized by a delayed IR pulse. The resulting energy- and angular-resolved photoelectron spectra carry information about the

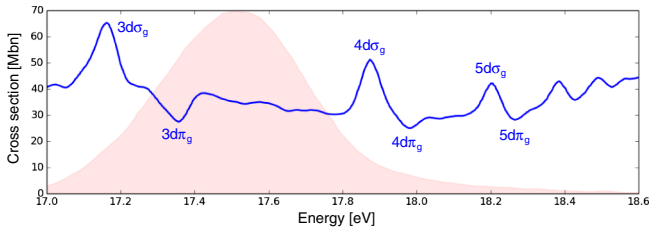

FIG. 1. N_2 photoabsorption cross section [19]. The XUV pulse spectrum is plotted as a pink shaded area (scaled for visibility). Labels for the $(B^2\Sigma_u^+)$'d'σ_g and $(B^2\Sigma_u^+)d\pi_g$ series are given following Ref. [16].

electronic structure and autoionization dynamics of the resonance. This allows us to identify two individual electronic states contributing to the resonance and to assess their lifetimes.

The experimental apparatus is described in detail elsewhere [5]. In brief, near-infrared pulses (2 mJ, 20 fs) are used to drive high-order harmonic generation in argon gas [17]. The resulting XUV radiation is spectrally filtered by a two-stage time-delay-compensating monochromator. The driving IR radiation is blocked by a thin Al filter (100 nm) to prevent IR leakage to the interaction region. The beam line parameters are tuned to produce an XUV pulse with a spectrum centered at 17.5 eV and a full width at half maximum (FWHM) of 0.5 eV (see Fig. 1) [18]. In this photon energy range the spectrum overlaps with the $3d\pi_g$ member of the Hopfield emission series [19]. The XUV radiation is focused at an effusive, room-temperature jet of nitrogen molecules. A second near-IR pulse (795-nm center wavelength, 90-nm bandwidth) with an energy of 50 μJ (intensity of 2 TW/cm^2 in the focus) is used to ionize the excited molecules before they decay via autoionization.

The photoelectron energy and angular distributions are recorded using a velocity map imaging (VMI) spectrometer [20]. In these experiments photoemission is cylindrically symmetric around the axis of linear polarization of both the XUV and the IR beams, which allows reconstruction of the 3D momentum distribution of the electrons using the BASEX algorithm [21].

A slice through the 3D photoelectron distribution generated by the XUV pulse only is shown in Fig. 2(a) as a false color plot. The outer ring corresponds to photoelectrons emerging in the $X^2\Sigma_g^+(\nu=0)$ ionization channel of N_2^+ (labeled X_0), where ν denotes the vibrational state of the molecular ion. The inner rings correspond to the $A^2\Pi_u(\nu=0,1,2)$ channels (labeled $A_{0,1,2}$). The kinetic energies of the features observed in Fig. 2 are given in Table I.

Overlap of an IR laser pulse with the XUV pulse induces new features in the photoelectron distributions. Figure 2(b) shows the difference between an image recorded with both the XUV and the IR pulses and one recorded with the XUV pulse only. Red and blue colors indicate a signal increase

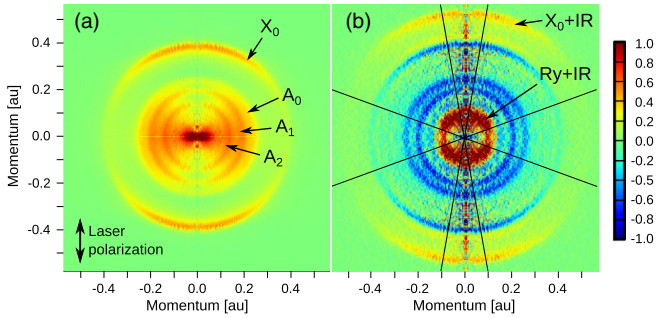

FIG. 2. (a) Slice through a 3D photoelectron momentum distribution resulting from ionization of N_2 molecules by the XUV pulse. The axes are given in atomic units of momentum (au). (b) Difference between distributions recorded with XUV + IR (zero time delay) and only XUV pulses. The IR-induced signal is scaled 20 times for visibility. The relative color scale for (a) and (b) is shown on the right. The double arrow indicates the direction of the laser polarization of both the XUV and IR pulses. Thin black lines show angular ranges used to extract angle-dependent signals (see text for details).

and depletion by the IR pulse, respectively. A new ring appears at higher kinetic energy, which corresponds to generation of the $n=+1$ sideband in the X_0 channel [23,24]. The kinetic energy of these photoelectrons is larger than the energy of the photoelectrons in the X_0 channel by exactly the energy of one IR photon (1.56 eV); this contribution is therefore labeled as $X_0+\mathrm{IR}$. Similar photoelectrons are generated for the $A_{0,1,2}$ states, but they overlap with the depletion of the X state. The sideband generation process can both increase and decrease the kinetic energy of the electron created by the XUV pulse. For the X_0 channel the signal corresponding to this $n=-1$ sideband overlaps with feature A_2. The kinetic energy in the $A_{0,1,2}$ channels is too low for inducing $n=-1$ sidebands in the photoelectron spectrum.

The kinetic energy of the strong signal close to the center of the image (labeled Ry + IR) corresponds to one-photon ionization of the resonant Rydberg state at 17.33 eV. We therefore conclude that the IR pulse is able to ionize the excited Rydberg states before they undergo autoionization.

TABLE I. Photoelectron kinetic energy E_k and angular asymmetry parameters β_2 for the features observed in XUV-only and XUV-IR spectra.

Label	E_k (eV)	β_2 (this work)	β_2 (Ref. [22])
X_0	2.0	0.94(4)	1.0
A_0	0.8	−0.35(2)	−0.3
A_1	0.55	−0.42(1)	−0.4
A_2	0.3	−0.48(2)	−0.5
$X_0+\mathrm{IR}$	3.5	1.7(2)	⋯
Ry + IR	0.18	0.3–2.0	⋯
Ry	1.75	⋯	⋯

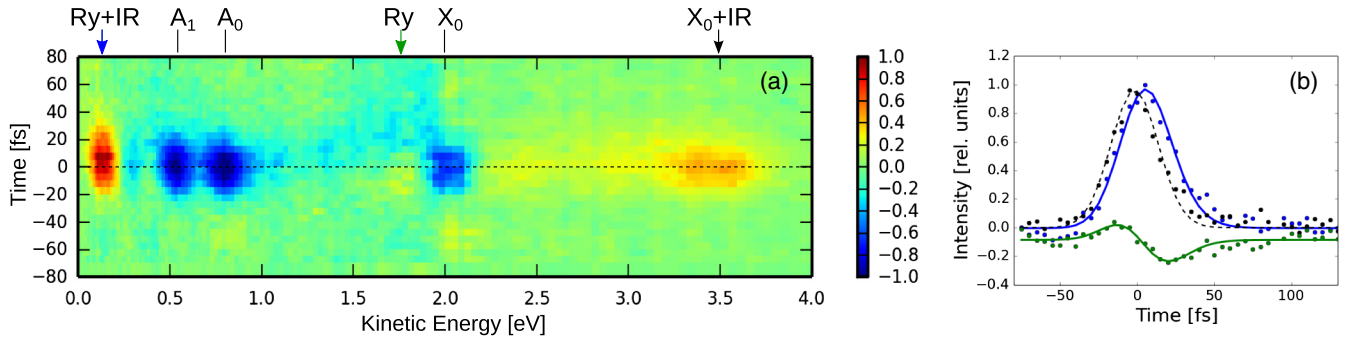

FIG. 3. (a) False color map of differential photoelectron kinetic energy distributions resulting from angular integration of the distributions of Fig. 2(b) recorded for a sequence of pump-probe delays. Features observed in the map are labeled on the top. The dashed line corresponds to the zero time delay extracted from the time dependence of the sidebands. (b) Transient signals of features labeled Ry + IR (blue), Ry (green), and X_0 + IR (black) extracted from the map in (a). The energy integration ranges are 0.25 eV, 0.4 eV, and 0.7 eV, respectively. The X_0 + IR signal represents the XUV + IR cross correlation and is scaled for visibility. The lines show model fits (see text for details).

To access the autoionization dynamics, the photoelectron spectra are recorded as a function of the XUV-IR pump-probe delay. Time-dependent kinetic energy spectra integrated over all angles are shown in Fig. 3(a) as a false color map. The maximum of the differential IR-induced signal constitutes about 5% of the XUV-only signal. Most of the features in the map show dynamics, which are symmetric with respect to time "zero" (dashed line), determined as the position of the maximum of the feature X_0 + IR. This is expected for direct ionization in the presence of the IR pulse [23,24]. However, the feature at 0.18 eV clearly extends in the direction of positive time delays (the IR pulse arriving after the XUV pulse). This behavior is expected for a state with a nonzero lifetime and, therefore, supports the assignment of this feature to ionization of an autoionizing Rydberg state. Another region with nontrivial dynamics is observed around 1.75 eV. At negative time delays the signal is positive, but it decreases and becomes negative at positive time delays. Based on the kinetic energy we assign the negative signal to a depletion of the autoionization signal into the X state of the ion. This feature is the counterpart of the Ry + IR feature observed at 0.18 eV; we therefore label it as the feature Ry.

The transient dynamics of the autoionization features in Fig. 3(a) are shown in Fig. 3(b) along with the cross-correlation signal obtained from the X_0 + IR sideband. The X_0 + IR feature is fitted to a Gaussian function (black dashed line) and used to calibrate the zero delay between the XUV and IR pulses and their cross-correlation FWHM of 36 ± 1 fs. The depletion of the X_0 state and the depletions in the A manifold are all well described by this cross-correlation width. The peak of the Ry + IR feature is clearly shifted in time with respect to the cross-correlation signal and has an exponential tail extending to positive time delays. In Fig. 3(b) it is fitted to a convolution of the Gaussian cross-correlation function and an exponential decay, which yields a decay time of 8.5 fs. As discussed above, the temporal profile of the feature Ry at 1.75 eV has a more complicated shape. The differential signal first increases, but then reaches a maximum and subsequently becomes negative at positive time delays. The feature is modeled by the sum of a positive Gaussian contribution attributed to a sideband in the A channel and a single exponential decay component with a negative amplitude describing the depletion of the Rydberg state by the IR pulse. The decay constant derived from this model is consistent with the one extracted from the Ry + IR transient within the errors of the fit.

The VMI images provide not only kinetic energy distributions, but also energy-dependent angular distributions for the transient autoionizing state we have identified above. Photoelectron angular distributions from unaligned molecules are described by asymmetry parameters β, which weigh the contributions of different spherical harmonics in the wave function of the emitted electron. For direct ionization by one XUV photon, one asymmetry parameter (β_2) is required. The values of β_2 extracted for the features X_0 and $A_{0,1,2}$ are given in Table I and correspond well to values found in the literature. In the case of ionization by two (XUV and IR) photons with linear polarizations, two parameters (β_2 and β_4) are required,

$$\sigma(\theta, E) = \frac{\sigma_0(E)}{4\pi}[1 + \beta_2(E)P_2(\cos\theta) + \beta_4(E)P_4(\cos\theta)], \quad (1)$$

where $\sigma(\theta, E)$ is the doubly differential cross section (in energy and in angle), $\sigma_0(E)$ is the angle-integrated cross section, P_2 and P_4 are the second- and fourth-order Legendre polynomials, respectively, E is the photoelectron kinetic energy, and θ is the polar angle.

The time-dependent asymmetry parameters of the feature Ry + IR are plotted in Fig. 4. The value of the asymmetry parameter β_2 increases with time delay from 0.3 to about 2,

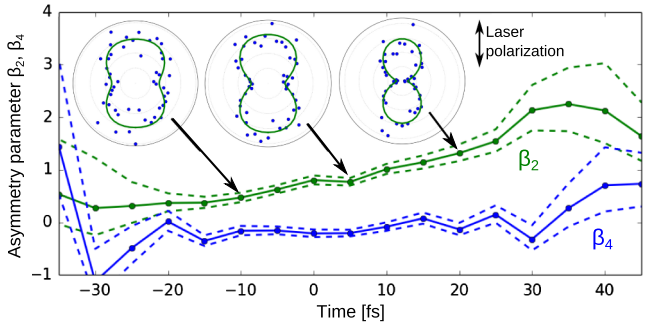

FIG. 4. Time-dependent asymmetry parameters β_2 and β_4 for the feature Ry + IR extracted from the full angular distributions in the differences of VMI images [Fig. 2(b)]. The analysis is sensitive to the background subtraction method, which can yield small systematic deviations. To evaluate the effect of the background, two images of the sequence—one at large positive time delays and one at large negative time delays—are used as XUV-only background to calculate the difference VMI images. The two resulting asymmetry parameters are plotted as dashed lines, showing that between −15 and 30 fs the results are robust against changes in the subtraction procedure. The insets show the photoelectron angular distributions as polar plots for the time delays indicated by arrows. The solid lines in the insets are fits using Eq. (1).

whereas parameter β_4 has a small negative value and is relatively constant. Larger values of β_2 correspond to angular distributions peaked along the polarization axis. This can be clearly seen in the angular distributions for three time delays plotted in Fig. 4 as insets. We argue that the time dependence of the asymmetry of the feature Ry + IR indicates that there is more than one electronic state contributing to its signal.

To take a further look, normalized transients of feature Ry + IR integrated within narrow angular ranges [shown in Fig. 2(b)] parallel and perpendicular to the laser polarization are plotted in Fig. 5. Consistent with the increase of β_2, the signal in the parallel direction shows slower dynamics leading to photoemission strongly peaked along the laser polarization for positive time delays. This transient can be modeled by an exponential decay with a time constant of

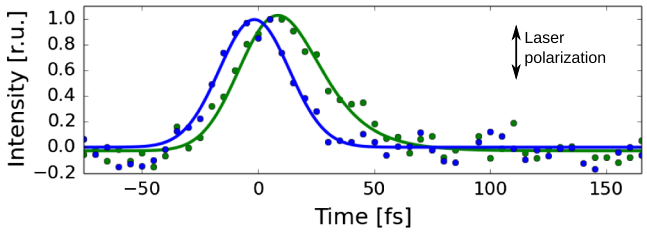

FIG. 5. Transient signals of the feature Ry + IR integrated parallel (green) and perpendicular (blue) to the laser polarization in the angular ranges indicated in Fig. 2(b). The solid lines are least-square fits to a convolution of the cross-correlation function and an exponential decay (see text).

14 ± 1 fs. The signal in the perpendicular direction coincides, within the experimental accuracy, with the XUV-IR cross-correlation function. The latter suggests that the second transient is very fast and cannot be resolved in the present experiment. The fits are shown in Fig. 5 as solid lines.

We proceed to discuss possible origins of the two contributions observed in the time-dependent angular distribution of the feature Ry + IR. As described above, the contribution along the laser polarization has a lifetime of about 14 fs, while the perpendicular one is only visible during the overlap of the XUV and IR pulses. In principle, two processes are possible at the observed photoelectron kinetic energy, namely, XUV + IR ionization in the B channel and XUV-IR ionization ($n = -1$ sideband) in the X channel. However, since one-photon photoemission in both the X and B channels is known to peak along the laser polarization [25] and both XUV and IR pulses are linearly polarized in the same direction, we expect that the nonresonant two-photon process should also lead to signals peaking along the laser polarization. This contradicts our observations and forces us to exclude nonresonant processes as the cause of the observed transient.

Turning to resonant excitation processes, we recall that two Rydberg states can be present in the energy window probed by our XUV pulse, namely, the $(B^2\Sigma_u^+)4's'\sigma_g$ state and the $(B^2\Sigma_u^+)3d\pi_g$ state. We propose that the Hopfield emission resonance is indeed composed of two superimposed Rydberg states, which we can distinguish by their lifetimes. This assignment is in agreement with the calculations of Raoult *et al.* [16] and indicates that the Rydberg series suggested by Ogawa and Tanaka [7] indeed exists in this photon energy range, but is masked by the Hopfield emission series and interacts with it via continuum coupling. The effect of mixing of resonances via continuum couplings is in fact well established. It was first considered by Mies, who demonstrated that overlapping Rydberg states lead to absorption spectra with complex shapes [26]. This is also similar to the effect of interference stabilization [27] or interference narrowing [28] for Rydberg atoms in strong (laser) electric fields.

In their review (and in references therein), Popov and coworkers [27] demonstrate that a system of two discrete resonances coupled to a continuum and having overlapping widths can transform into a system of two resonances located at the same energy, one of them being narrow (long lifetime) and one broad (short lifetime). This so-called interference stabilization happens when the widths of the resonances are larger than the energy gap between them. The only difference between the system of Ref. [27] and the one considered here is the origin of the continuum coupling (laser-induced vs multielectronic coupling, respectively).

The calculations of Raoult *et al.* yield a separation between the $(B^2\Sigma_u^+)4's'\sigma_g$ and $(B^2\Sigma_u^+)3d\pi_g$ states of about 40 meV, smaller than the widths of about 60 meV for both

resonances (estimated from Ref. [16]). Thus, the condition for interference stabilization is fulfilled. The Rydberg states in our case are thus expected to merge and form a pair of states with long and short lifetimes, similar to the experimental observations presented here. Fine details of this effect sensitively depend on the energy separation and widths of the underlying Rydberg states and require more detailed calculations than those presented in Ref. [16].

In conclusion, this manuscript presents an experimental investigation of the autoionization dynamics in N_2 molecules using time-, energy-, and angular-resolved photoelectron spectroscopy. The unique capabilities provided by an XUV time-delay-compensating monochromator beam line [5] allow us to investigate an autoionizing resonance with a time resolution short enough to observe the autoionization dynamics. The autoionizing states are promptly ionized by a weak IR probe pulse and the resulting photoelectron angular distributions change as a function of pump-probe delay, which allows us to decompose the resonance into two components with preferential photoemission in mutually perpendicular directions.

The component along the laser polarization shows an exponential decay of 14 ± 1 fs, while the component perpendicular to the laser polarization has a lifetime below the experimentally detectable limit. This observation and an analysis of available theoretical calculations suggests that the electronic states are influenced by the phenomenon of interference stabilization [27] and that their lifetimes are determined by interference effects in the continua, to which both states are coupled.

The authors thank Misha Ivanov for bringing to their attention the effect of interference stabilization. They thank Lukas Medisauskas and Serguei Patchkovskii for helpful discussions and Maurizio Reduzzi for providing the data for the XUV absorption spectrum.

*kornilov@mbi-berlin.de

[1] U. Fano, Phys. Rev. **124**, 1866 (1961).
[2] H. Wang, M. Chini, S. Chen, C.-H. Zhang, F. He, Y. Cheng, Y. Wu, U. Thumm, and Z. Chang, Phys. Rev. Lett. **105**, 143002 (2010).
[3] C. Ott, A. Kaldun, P. Raith, K. Meyer, M. Laux, J. Evers, C. H. Keitel, C. H. Greene, and T. Pfeifer, Science **340**, 716 (2013).
[4] H. Mashiko, T. Yamaguchi, K. Oguri, A. Suda, and H. Gotoh, Nat. Commun. **5**, 5599 (2014).
[5] M. Eckstein, C.-H. Yang, M. Kubin, F. Frassetto, L. Poletto, H.-H. Ritze, M. J. J. Vrakking, and O. Kornilov, J. Phys. Chem. Lett. **6**, 419 (2015).
[6] J. J. Hopfield, Phys. Rev. **35**, 1133 (1930).
[7] M. Ogawa and Y. Tanaka, Can. J. Phys. **40**, 1593 (1962).
[8] K. P. Huber, G. Stark, and K. Ito, J. Chem. Phys. **98**, 4471 (1993).
[9] P. Gürtler, V. Saile, and E. Koch, Chem. Phys. Lett. **48**, 245 (1977).
[10] E. W. Plummer, T. Gustafsson, W. Gudat, and D. E. Eastman, Phys. Rev. A **15**, 2339 (1977).
[11] P. R. Woodruff and G. V. Marr, Proc. R. Soc. A **358**, 87 (1977).
[12] A. C. Parr, D. L. Ederer, B. E. Cole, J. B. West, R. Stockbauer, K. Codling, and J. L. Dehmer, Phys. Rev. Lett. **46**, 22 (1981).
[13] P. M. Dehmer, P. J. Miller, and W. A. Chupka, J. Chem. Phys. **80**, 1030 (1984).
[14] P. Croteau, J. B. Randazzo, O. Kostko, M. Ahmed, M.-C. Liang, Y. L. Yung, and K. A. Boering, Astrophys. J. Lett. **728**, L32 (2011).
[15] M. Sommavilla, U. Hollenstein, G. M. Greetham, and F. Merkt, J. Phys. B **35**, 3901 (2002).
[16] M. Raoult, H. L. Rouzo, G. Raseev, and H. Lefebvre-Brion, J. Phys. B **16**, 4601 (1983).
[17] T. Pfeifer, C. Spielmann, and G. Gerber, Rep. Prog. Phys. **69**, 443 (2006).
[18] The XUV photon energy is calibrated by measuring kinetic energy distributions of photoelectrons resulting from ionization of Ar atoms.
[19] M. Reduzzi, W.-C. Chu, C. Feng, A. Dubrouil, J. Hummert, F. Calegari, F. Frassetto, L. Poletto, O. Kornilov, M. Nisoli, C. D. Lin, and G. Sansone, J. Phys. B **49**, 065102 (2016).
[20] O. Ghafur, W. Siu, P. Johnsson, M. F. Kling, M. Drescher, and M. J. J. Vrakking, Rev. Sci. Instrum. **80**, 033110 (2009).
[21] V. Dribinski, A. Ossadtchi, V. A. Mandelshtam, and H. Reisler, Rev. Sci. Instrum. **73**, 2634 (2002).
[22] J. B. West, K. Codling, A. C. Parr, D. L. Ederer, B. E. Cole, R. Stockbauer, and J. L. Dehmer, J. Phys. B **14**, 1791 (1981).
[23] N. M. Kroll and K. M. Watson, Phys. Rev. A **8**, 804 (1973).
[24] A. Maquet and R. Taïeb, J. Mod. Opt. **54**, 1847 (2007).
[25] M. Ilchen, S. Deinert, L. Glaser, F. Scholz, J. Seltmann, P. Walter, and J. Viefhaus, J. Phys. B **45**, 225102 (2012).
[26] F. H. Mies, Phys. Rev. **175**, 164 (1968).
[27] A. M. Popov, O. V. Tikhonova, and E. A. Volkova, J. Phys. B **36**, R125 (2003).
[28] A. S. Stodolna, F. Lépine, T. Bergeman, F. Robicheaux, A. Gijsbertsen, J. H. Jungmann, C. Bordas, and M. J. J. Vrakking, Phys. Rev. Lett. **113**, 103002 (2014).